Formation of zinc oxide films using submicron zinc particle dispersions

Meena S. Rajachidambaram
School of Chemical, Biological and Environmental Engineering, Oregon State University, Corvallis, Oregon 97331

Tamas Varga, Libor Kovarik, Rahul Sanghavi, Vaithiyalingam Shutthanandan, and Suntharampillai Thevuthasan
Environmental Molecular Sciences Laboratory, Pacific Northwest National Laboratory, Richland, Washington 99354

Seung-Yeol Han, Chih-Hung Chang, and Gregory S. Herman[a)]
School of Chemical, Biological and Environmental Engineering, Oregon State University, Corvallis, Oregon 97331

(Received 27 January 2012; accepted 29 May 2012; published 27 June 2012)

The thermal oxidation of submicron metallic Zn particles was studied as a method to form nanostructured ZnO films. The particles used for this work were characterized by electron microscopy, x ray diffraction, and thermal analysis to evaluate the Zn-ZnO core shell structure, surface morphology, and oxidation characteristics. Significant nanostructural changes were observed for films annealed to 400 °C or higher, where nanoflakes, nanoribbons, nanoneedles, and nanorods were formed as a result of stress induced fractures arising in the ZnO outer shell due to differential thermal expansion between the metallic Zn core and the ZnO shell. Mass transport occurs through these defects due to the high vapor pressure for metallic Zn at temperatures above 230 °C, whereupon the Zn vapor rapidly oxidizes in air to form the ZnO nanostructures. The Zn particles were also incorporated into zinc indium oxide precursor solutions to form thin film transistor test structures to evaluate the potential of forming nanostructured field effect sensors using simple solution processing. © *2012 American Vacuum Society*. [http://dx.doi.org/10.1116/1.4731255]

I. INTRODUCTION

Zinc oxide (ZnO) is an economical and environmentally benign transparent wide bandgap (3.37 eV) semiconductor with a number of interesting chemical, electrical, piezoelectrical, and optical properties, making it uniquely suited for a variety of thin-film device applications.[1] For example, ZnO has been used in gas sensors,[2,3] photodiodes,[4] varistors,[5] piezoelectric devices,[3] and thin film transistors (TFTs).[1,6] Typically ZnO films are deposited by vacuum-based methods which include sputter deposition,[7,8] electron-beam evaporation,[9] thermal evaporation,[10] chemical vapor deposition,[11] and atomic layer deposition.[12] To produce films at potentially lower costs, efforts have focused on solution-based methods, including sol-gel[13,14] and oxide nanoparticle dispersions.[1,6,15]

Recently, research has focused on using solution-processed ZnO as the active material for TFTs. ZnO nanoparticle approaches have been investigated by several groups, where stable dispersions of ZnO nanoparticles have been deposited and subsequently annealed.[16] Studies found that it was necessary to anneal the nanoparticle ZnO films up to 500 °C in air to remove surface impurities including hydroxyls, and to obtain good TFT performance where mobilities as high as 0.104 cm^2/V s could be obtained. An issue with the nanoparticle approach is that high temperatures are necessary to increase grain size and density of the films, and this may limit its applicability for low-temperature processing for flexible electronics on polymeric substrates. Another approach to form ZnO films at lower temperatures is to form stable molecular precursors. For example, Meyers *et al*. have recently produced dense, high quality polycrystalline ZnO films by inkjet printing and spin coating for channel layer in TFTs.[17] It was found that large grain ZnO films were formed after post-annealing the printed films to 300 °C or spin-coated films to 150 °C. The resulting devices fabricated using printed films demonstrated good electronic properties with incremental mobilities of 4–6 cm^2/V s, while the devices with spin-coated films showed incremental mobilities of 1.8 cm^2/V s. Low-temperature processed ZnO films have also been demonstrated by Cheng *et al*., where bottom gate ZnO TFTs were fabricated using chemical bath deposition from a zinc nitrate precursor at 60 °C which was then dried at 100 °C with no further annealing.[18] These devices had a channel mobility of 0.248 cm^2/V s.

Another interesting property of ZnO is the wide variety of nanostructures that have been formed with different morphologies such as nanorods,[1,15,19] nanoneedles,[20,21] nanowires,[3,20,21] nanobelts,[3,22] and nanoflakes.[23] Recently it has been demonstrated that nanostructured ZnO films can be formed by the thermal oxidation of Zn nanoparticle films.[7,9] For example, Kim *et al*. deposited Zn nanowires by RF magnetron sputtering and fabricated coaxial Zn/ZnO nanocables by thermal oxidation between 100 °C and 400 °C. These studies indicated that controlled thermal oxidation of Zn nanowires can substantially modify the Zn/ZnO core-shell structures.[7] Alivov *et al*. also reported that thermal oxidation of Zn films, deposited by electron-beam evaporation, can have a significant impact on film properties including roughness, resistivity, mobility, and luminescence.[9] It is fairly

[a)]Author to whom correspondence should be addressed; electronic mail: greg.herman@oregonstate.edu

Downloaded 14 Sep 2012 to 128.193.163.10. Redistribution subject to AVS license or copyright; see http://avspublications.org/jvstb/about/rights_and_permissions

common to find oxide shells on the surface of metal particles, and for Zn the ZnO shell can significantly influence the electrical, chemical, and physical properties of the particle. Furthermore, it has been shown that the method used to form the ZnO shell can strongly influence the oxidation of Zn particles.[23] For example, Gui *et al*. have investigated the formation of nanostructures on Zn nano- and microparticles by a two-step oxidation process where preoxidation with H_2O_2 at different Zn/H_2O_2 ratios was followed by thermal oxidation.[23] For nanoparticles the simultaneous melting and oxidation of zinc led to the formation of nanostructures during the thermal oxidation step, while for microparticles the oxidation process began only after the melting of zinc.

In this paper we present results on the thermal oxidation of films formed by spin-coated submicron zinc particles. The Zn particles were characterized using thermogravimetric analysis (TGA), transmission electron microscopy (TEM), helium ion microscopy (HIM), and x ray diffraction (XRD). The Zn particles were incorporated into zinc indium oxide (ZIO) solutions to form test structures to evaluate the potential of forming nanostructured field-effect sensors.

II. EXPERIMENTAL METHODS

Zn particles with vendor specified average diameters of 35 and 130 nm were purchased from Nanostructured and Amorphous Materials, Inc. The particles were stored in an inert environment prior to formation of dispersions to minimize exposure to oxygen (O_2) and water vapor (H_2O) and the resulting incidental oxidation.

A TA Instruments modulated TGA 2950 was used for thermogravimetric analysis of the Zn particles. Analysis was performed using ~25 mg of the particles, an airflow rate of 60 cm^3/min, and a heating rate of 5 °C/min up to 600 °C, with an isothermal step at 150 °C for 10 min.

A Carl Zeiss SMT ORION Plus HIM was used to obtain images of the Zn particles before and after annealing the samples to characterize thermally induced structural changes. Images of the un-annealed films were obtained using HIM to investigate the film morphology and to analyze the particle size distribution. Using ImageJ 1.45I software, the size distributions of the particles were determined to be 162 ± 86 nm and 234 ± 112 nm for the vendor specified 35 and 130 nm, respectively.

A Rigaku D/Max Rapid II micro-x ray diffraction (micro-XRD) system was used to characterize the crystallographic phase and composition ratio of Zn:ZnO. The micro-XRD has a rotating Cr anode ($\lambda = 2.2897$ Å) with an operating power of 875 W, where a 0.3 mm collimator was used to define the analysis area. The data analysis was performed using Jade 9.1.5 (Materials Data, Inc.) software to determine the crystallographic phase and the relative composition of the Zn particles (e.g., Zn metal and ZnO).

A JOEL TEM 2010 system operated at 200 kV was used to obtain TEM images of the Zn particles. The images were obtained using a low electron dose to minimize beam-induced damage. The samples were prepared by depositing the particles onto carbon coated TEM grids after annealing in air.

Stable dispersions of ~5 wt. % Zn particles were prepared by adding 1.0 g of Zn particles into a 1:3 volume ratio of methanol:chloroform.[15] Approximately 0.35 ml of either n-octylamine or n-ethylmethylamine was added as a dispersant and the solutions were sonicated using a Branson digital sonifier 450 model ultrasonic probe. Typically the sonifier was operated at 400 W and 50% amplitude for ~30 min to break up particle agglomerations. During ultrasonication the vials were placed in an ice bath to minimize heating of the solutions and evaporation of volatile solvents. The resulting dispersions were found to be stable for several days.

The dispersions were spin-coated at 500 rpm for 30 s on thermally oxidized Si substrates (100 nm SiO_2). Prior to coating, the substrates were O_2 plasma treated to remove residual organics and then exposed to hexamethylene disilazane vapor to create a hydrophobic surface.[15] Film thicknesses were determined to be ~1.5 to ~2.5 μm, as by profilometry and scanning electron microscopy cross-sections. Films were then annealed in a tube furnace for 1 h in air at 100 °C, 200 °C, 300 °C, 400 °C, 500 °C, or 600 °C using a ramp rate of 7 °C/min.

To form semiconducting ZIO films that incorporate Zn particles, we prepared ZIO precursors using indium chloride ($InCl_3$) and zinc chloride ($ZnCl_3$) dissolved in acetonitrile (0.025 M $InCl_3$/$ZnCl_3$),[24] where ethylene glycol (EG) was added (1:50 EG:acetonitrile volume ratio) to increase solution viscosity and decrease the evaporation rate.[25] Finally, Zn particles were added to the ZIO solution to obtain a Zn particle loading of 5 wt. %.

The resistivity (ρ) of the annealed films were measured using a Jandel model RM2 four point probe where the current, I, was set to 0.1 μA and voltage, V (mV), was measured to determine the resistivity with respect to thickness, t (cm), of the films using the relation

$$\rho = [\pi \times \mathrm{t} \times \mathrm{V}]/[\ln(2) \times \mathrm{I}].$$

A set of TFT test structures were fabricated with channel layers formed by spin-coating ZIO that did not contain Zn particles followed by the 5 wt. % solutions of ZIO with both Zn particle sizes. The spin coating was carried out at 3000 rpm for 30 s on Si/SiO_2 substrates. Prior to spin coating, the substrates were made hydrophilic by ultrasonicating in a 1 M NaOH solution. Film thickness was ~600 nm as determined by profilometry. These films were annealed to 400 °C, 500 °C, or 600 °C in air for 2 h. Patterning was performed using photolithography, where a 0.5 mM HCl etchant was used to pattern the Zn particle layer followed by an oxalic acid etchant to pattern the underlying ZIO layer. The test structures were completed by evaporating 500 nm Al through a shadow mask to form source-drain contacts. A schematic of the test structure is shown in Fig. 1. Another batch of TFT test structures with only the spin-coated ZIO solution processed under identical conditions were used as reference devices.

III. RESULTS AND DISCUSSIONS

In Fig. 2 we show thermogravimetric data for the Zn particles to identify the onset of oxidation, the temperature

Downloaded 14 Sep 2012 to 128.193.163.10. Redistribution subject to AVS license or copyright; see http://avspublications.org/jvstb/about/rights_and_permissions

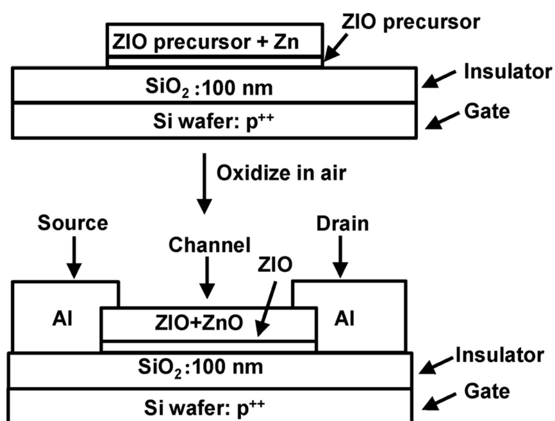

FIG. 1. Structure of a bottom-gate TFT test structure in which the Zn particles are deposited by spin-coating and then oxidized to ZnO by annealing in air.

at which the particles are completely oxidized, and their respective mass gains. There is a significant mass increase starting at ∼250 °C, which can be attributed to the oxidation of the Zn particles. By 500 °C there was no further increase in mass, suggesting that Zn particles were completely oxidized, where a mass gain of 15.1% and 19.4% was obtained for the 162 and 234 nm diameter particles, respectively. These values can be compared to the expected mass gain for Zn to ZnO, which is 24.5%, suggesting that the smaller zinc particles initially have a larger relative ratio of ZnO to Zn compared to the larger particles. This is not unexpected since there should be the presence of native oxide and the thickness should be independent for the particle sizes under investigation, where the larger particles will have a larger volume of Zn compared to the volume of the ZnO shell leading to a higher mass gain.

HIM images of the spin-coated Zn particle films annealed at different temperatures are shown in Figs. 3(a)–3(n). As can be seen, the films formed from 162 nm diameter particles had minimal structural changes for annealing temperatures below 400 °C. However, for 400 °C anneals significant coalescence of the particles begins, and after annealing to 500 °C and 600 °C a variety of nanostructures are observed. We found that larger particles initially had structural changes

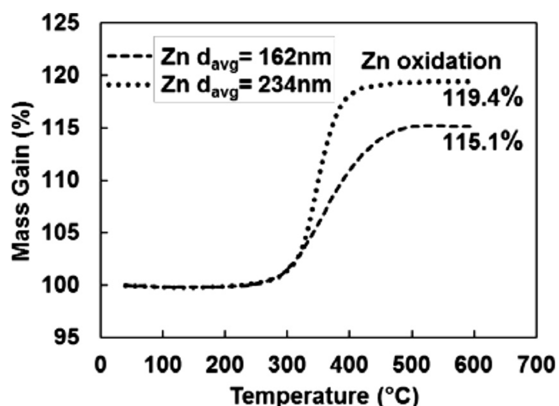

FIG. 2. TGA of Zn particles with $d_{avg} = 162$ and 234 nm.

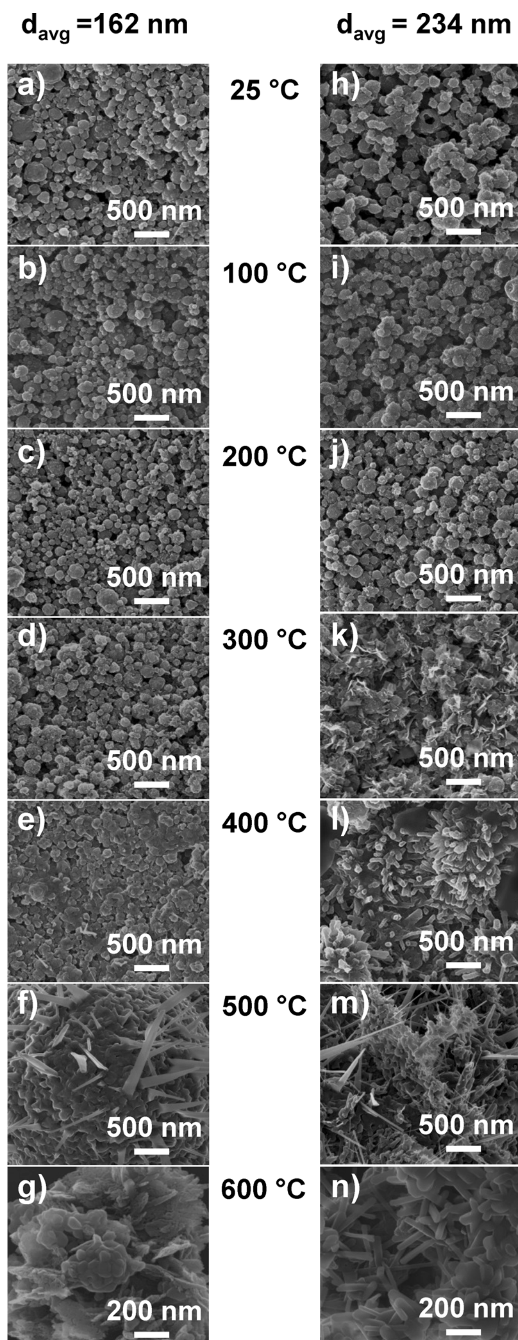

FIG. 3. Helium ion microscope images of Zn particle films, $d_{avg} = 162$ nm (a)–(g) and $d_{avg} = 234$ nm (h)–(n), that have been spin-coated and annealed to the indicated temperatures.

beginning at 300 °C, and showed similar variable morphology for anneal temperatures 400 °C and higher, including the formation of nanoribbons, nanoneedles, and nanorods. These nanostructures were primarily formed in specific regions of the films, which may be related to regions with initially larger Zn particles.

The formation of ZnO nanostructures due to thermal oxidation of Zn nano- and micron sized particles has been demonstrated previously in the literature.[7,21,23,26–32] Several different models have been proposed for the formation of ZnO nanostructures by the thermal oxidation of zinc. For

Downloaded 14 Sep 2012 to 128.193.163.10. Redistribution subject to AVS license or copyright; see http://avspublications.org/jvstb/about/rights_and_permissions

example, prior studies have proposed that nanorod formation from the oxidation of Zn particles is related to a variety of factors including the sublimation of zinc, the reaction of zinc atoms and clusters with oxygen in air, and the deposition of these atoms and clusters onto the surface of the particles, resulting in the growth of nanostructures in preferred growth directions for ZnO.[7,21] Other studies have indicated that the Zn/ZnO core-shell structure participates in the formation of ZnO nanostructures, where high stress forms at elevated temperatures due to the large difference in thermal expansion coefficients of Zn (60.8×10^{-6}/deg) and ZnO (4×10^{-6}/deg).[23,28] This large amount of stress causes the ZnO outer shell to fracture, whereupon the evaporation of metallic zinc occurs through these fractures, and this Zn vapor is rapidly oxidized by air, resulting in the formation of the ZnO nanostructures. Finally, it has also been proposed that the growth of the ZnO shell follows Cabrera and Mott mechanistics where the field formed from the absorption of oxygen on the surface drives the migration of ions through the thin oxide films.[32] It is believed that Zn ions are the dominant species that diffuse through the oxide film at low temperatures, and that enhanced diffusion of Zn ions at grain boundaries may lead to the preferential growth of ZnO nanostructures at specific locations on the Zn particles.[32]

In Figs. 4(a) and 4(b) we show XRD spectra obtained for Zn particle films annealed to the indicated temperatures. The diffraction patterns can be indexed to hexagonal Zn and wurtzite ZnO as indicated by the dashed and solid lines, respectively, at the bottom of the figures. Significant changes in the XRD patterns can be seen for the films upon annealing where a transition from the metal to oxide phase occurs between 300 °C and 400 °C. XRD patterns from unannealed Zn films are dominated by peaks corresponding to metallic Zn, but have low intensity peaks corresponding to ZnO, suggesting the presence of a crystalline native oxide shell on the Zn particles even prior to annealing. Peaks corresponding to ZnO are less intense for annealing temperatures up to 300 °C, before gradually increasing for temperatures between 300 °C and 400 °C and becoming quite prominent for 400 °C and 500 °C, as shown by the intense peak corresponding to the (101) plane of ZnO. Likewise, peaks corresponding to Zn show high intensity for annealing temperatures up to 300 °C, decreasing for 400 °C, and ultimately disappearing for 500 °C, as shown by the intense peak corresponding to the (101) plane of Zn metal. The peak at $2\theta = 88.72°$ in the XRD plot for larger particle films annealed to 600 °C corresponds to the Si (311) peak from the substrate. These data suggest that the complete oxidation of Zn to ZnO occurs between 400 °C and 500 °C. Furthermore, films formed from 162 and 234 nm diameter Zn particles had similar behavior, but with slight variations in relative intensities.

Quantitative phase analysis was performed to estimate the relative compositions of Zn and ZnO in the films. We analyzed the full diffraction patterns using the crystal structures for Zn (powder diffraction file #01-071-3764) and ZnO (powder diffraction file #01-074-9939) from the inorganic crystal structure database. The gradual decrease in metallic Zn composition and accompanying increase in ZnO composition for increasing annealing temperature is shown in Fig. 5. The initial un-annealed Zn:ZnO weight percent ratio was determined to be 70.1%:29.9% for the smaller diameter particles and 76.9%:23.1% for larger diameter particles. This indicates that films with larger particles have a larger metallic component than smaller particles, which is consistent with the TGA analysis described above. It was observed that the films with smaller diameter particles completely oxidized to ZnO at 500 °C, whereas the films with larger diameter particles required 600 °C for the complete oxidation of Zn (e.g., the XRD peaks for metallic Zn were still observed after

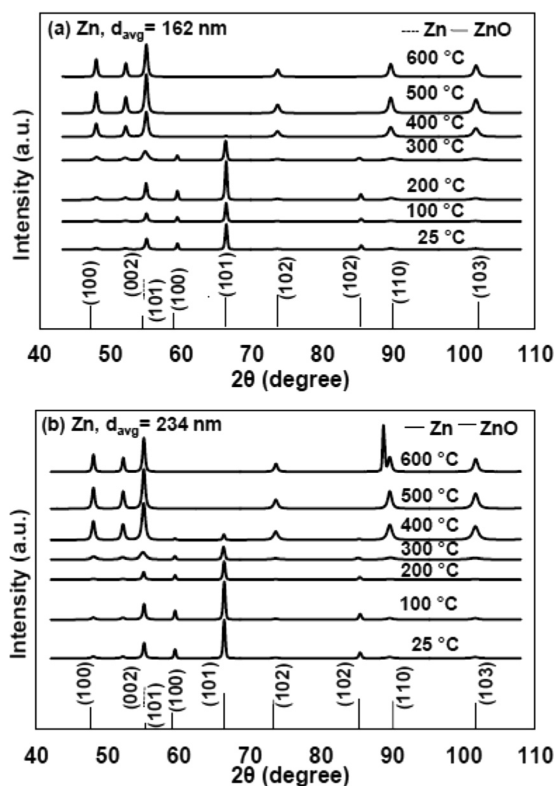

FIG. 4. X-ray diffraction results for (a) Zn particles, $d_{avg} = 162$ nm, and (b) Zn particles, $d_{avg} = 234$ nm, that have been annealed to the indicated temperatures.

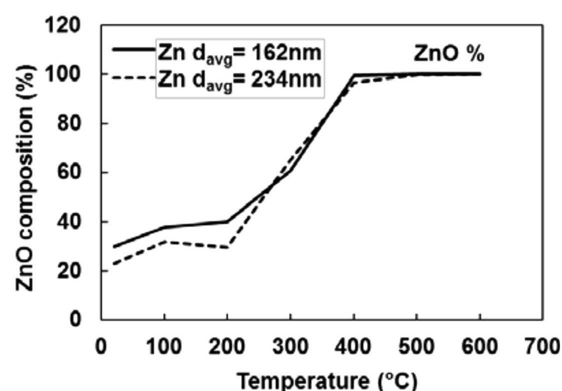

FIG. 5. Zn-ZnO weight percent composition as determined by micro-XRD for Zn particles with $d_{avg} = 162$ and 234 nm after annealing to the indicated temperatures.

Downloaded 14 Sep 2012 to 128.193.163.10. Redistribution subject to AVS license or copyright; see http://avspublications.org/jvstb/about/rights_and_permissions

annealing to 500 °C). The ZnO weight percent obtained at each temperature was used to estimate the percent mass gain for the 162 and 234 nm diameter Zn particles which were determined to be 10.0% and 14.3%, respectively, which compares reasonably well with the experimental mass gains determined from the TGA data.

From this data we have also estimated the thicknesses of the average ZnO shells for varying temperatures in Fig. 6. For these calculations, the particles are assumed to be spherical, where the initial diameters of the particles, as obtained by HIM, are taken to be 162 and 234 nm. These values include both the diameter of the Zn core and twice the thickness of the ZnO shell. When the weight percent values from the XRD data is combined with the particles' diameters, it can be determined that the smaller particles have a Zn core diameter of 123 nm and a ZnO shell thickness of 19 nm. Likewise, the larger particles have a Zn core diameter of 190 nm and a ZnO shell thickness of 22 nm. To estimate the thickness of the ZnO shell for the annealed samples we used the changes in weight percent for the Zn and ZnO, obtained using micro-XRD, after annealing to the various temperatures. These data provide both the volume of the Zn core and the ZnO shell, which can then be converted to the thickness of the ZnO shell.

In Fig. 7 we show TEM images of the 162 nm diameter Zn particles before and after annealing to the indicated temperatures in air. In the images there is a clear distinction between light and dark regions in the TEM, which can be correlated to changes in composition. In Fig. 7(a) the dark contrast is due to the Zn core of the particle, while the light contrast is due to the ZnO outer shell. In the inset is a high resolution image that clearly shows lattice fringes indicating that the ZnO on the particle is crystalline, even with no anneal. Selected area electron diffraction of the light regions confirms that these are due to a ZnO layer. After annealing to 300 °C it can be seen in Fig. 7(b) that the smaller nanoparticles become completely oxidized and can form hollow spheres, where some of the larger Zn particles still have dark regions corresponding to Zn cores with ZnO shells. With further annealing to 400 °C it can be seen in Fig. 7(c) that all the Zn particles are now completely oxidized, resulting in hollow spheres that are composed of multiple ZnO crystals.

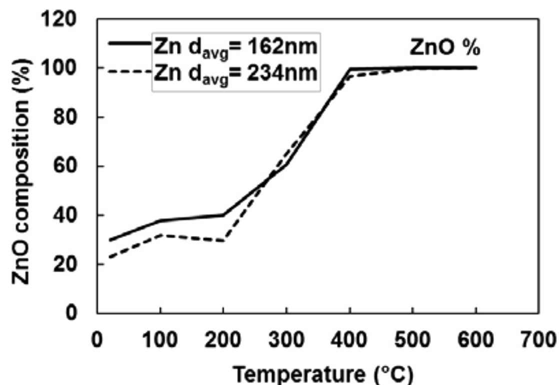

FIG. 6. Calculated thicknesses of ZnO outer shells for Zn particles with d_{avg} = 162 and 234 nm vs annealing temperature.

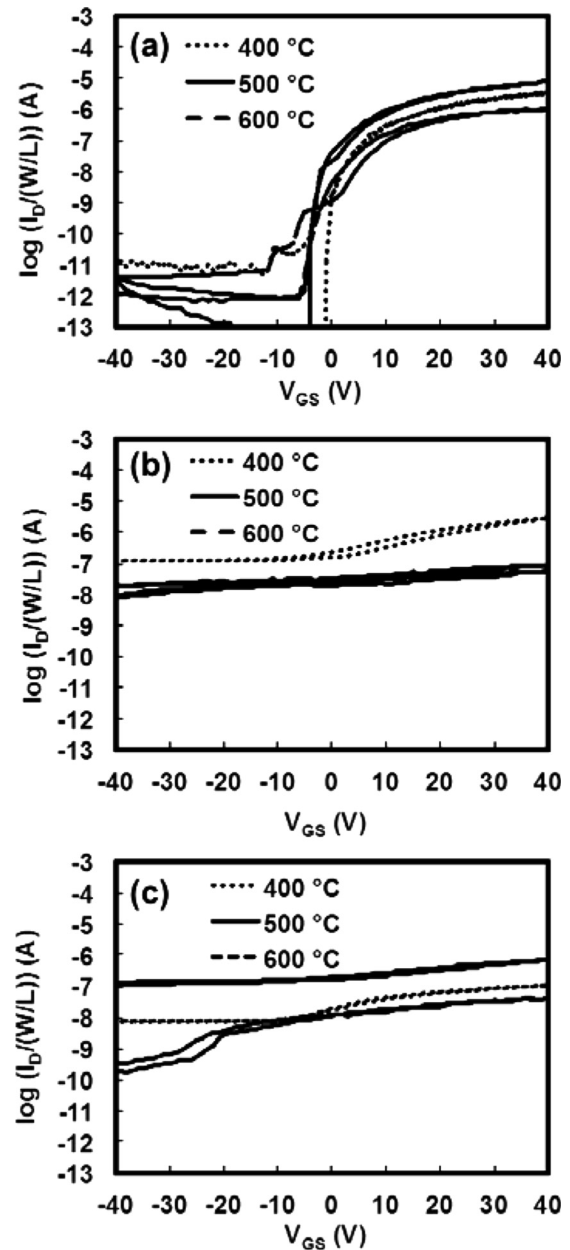

FIG. 7. TEM images for Zn particles with d_{avg} = 162 nm for (a) unannealed, (b) 300 °C annealed, and (c) 400 °C annealed samples. The inset in (a) shows HRTEM indicating atomic planes associated with ZnO for structures formed on the Zn particles.

Hollow ZnO spheres have been previously observed for Zn particles that have been annealed to various temperatures. In these studies it was proposed that Zn can diffuse out of defects formed in the ZnO shell during the annealing process.[26,29] Finally, in our analysis of the XRD data it should be noted that the ZnO shell is not completely uniform but are multicrystalline according to the TEM data. These multicrystalline ZnO shells are more likely to provide the defects necessary for the removal of Zn from the inside of the shell compared to homogeneous amorphous films and may help explain the formation of the hollow particles.

Film resistivity measurements using a 4-point probe are summarized in Table I. Films formed from the 162 nm

Downloaded 14 Sep 2012 to 128.193.163.10. Redistribution subject to AVS license or copyright; see http://avspublications.org/jvstb/about/rights_and_permissions

TABLE I. Resistivity measurements of Zn particle films, $d_{avg} = 162$ nm and Zn particles, $d_{avg} = 234$ nm, spin-coated using dispersions made up of chloroform/methanol and n-octylamine as a dispersant and after annealing at 300 °C, 400 °C, 500 °C, and 600 °C in air.

	Resistivity (Ω cm)	
Temperature (°C)	Zn $d_{avg} = 162$ nm	Zn $d_{avg} = 234$ nm
300	11.0	105.2
400	355.2	373.7
500	574.0	1059.7
600	658.8	1093.5

diameter Zn particles had a measured resistivity of ∼11 Ω cm after annealing to 300 °C, and increased to ∼350–650 Ω cm after annealing to 400–600 °C. In contrast, films formed from the 234 nm diameter particles had resistivity values of ∼105 Ω cm after annealing to 300 °C, and increased to nearly 1100 Ω cm after annealing to 500 °C and 600 °C. The reason for the low values of resistivity for 300 °C and 400 °C is likely due to the presence of a Zn core, whereas films annealed to 500 °C and 600 °C are almost completely oxidized (as indicated by the micro-XRD data) resulting in higher resistivities.

Thin film transistor test structures fabricated both with and without Zn particles, where the latter was used as a reference. The ZIO devices were annealed to 400 °C, 500 °C, and 600 °C and the transfer characteristics of the resulting devices are shown in Fig. 8(a), where the gate voltage (V_{GS}) was scanned from –40 to 40 V and back to –40 V with a fixed drain voltage (V_{DS}) of 1 V. The ZIO devices annealed to 400 °C, 500 °C, and 600 °C had turn on voltages (V_{ON}) of –7, 0, and –17 V, I_{on}/I_{off} ratios of ∼10^6, 10^7, and 10^5, and average mobilities (μ_{avg}) of 1.72, 1.78, and 0.71 cm^2/V s, respectively. Transfer characteristics, with the same V_{GS} range and V_{DS}, were obtained for devices that were formed with ZIO precursor containing Zn particles after a 400 °C anneal. For these devices we observed a combination of both conducting characteristics associated with Zn particles and semiconducting characteristics of the underlying ZIO layer, as shown in Figs. 8(b) and 8(c). For negative V_{GS} the channel conductance is dominated by the Zn particle films, due to the large thickness and the relatively low resistivities of these films. For positive V_{GS} the 400 °C films are observed to have field enhanced conduction, likely due to the semiconducting ZIO layer. Both particle based devices had V_{ON} of \tilde –10 V which is in good agreement with their corresponding reference devices. However, the I_{on}/I_{off} ratio was in the range of 10^1 to 10^2, which was much lower than that of the reference ZIO devices. The average mobilities on these devices could not be accurately calculated due to their high channel conductance. The I-V characteristics were also obtained for devices with particle films annealed to 500 °C and 600 °C. In the case of films with 162 nm diameter particles, the drain current versus gate voltage was nearly a straight line in the negative region for both 500 °C and 600 °C annealed devices. This suggests that the flow of current in the channel is dominated by the relatively low

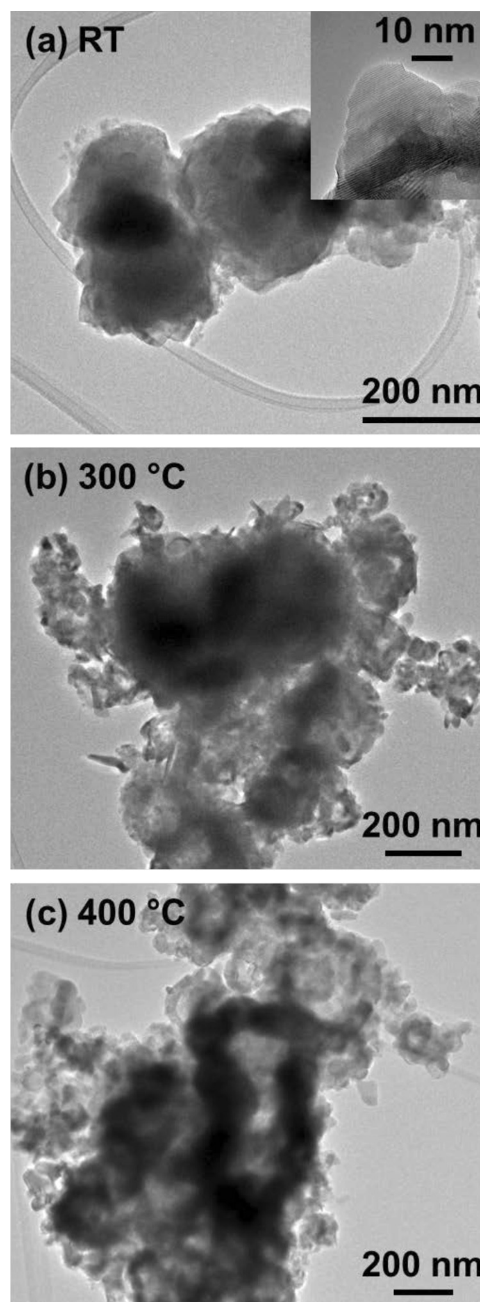

FIG. 8. Electrical characterization of TFTs deposited and annealed to 400 °C, 500 °C, and 600 °C by spin coating (a) ZIO films, (b) a bottom ZIO layer with 5% solution of $d_{avg} = 162$ nm Zn dispersed in ZIO, (c) a bottom ZIO layer with a 5% solution of $d_{avg} = 234$ nm Zn dispersed in ZIO.

resistivity of the ZnO films, which was confirmed by the associated four-point probe measurements. The films with 234 nm diameter particles had similar characteristics. Since there were no well-defined I_{on}/I_{off} characteristics, the V_{ON}, average mobility, and I_{on}/I_{off} ratio could not be determined.

IV. CONCLUSIONS

In this paper, we reported on a method for obtaining nanostructured ZnO films via thermal oxidation of spin-coated metallic Zn particles with average diameters of 162 and 234 nm, respectively. Thermal characterization using

Downloaded 14 Sep 2012 to 128.193.163.10. Redistribution subject to AVS license or copyright; see http://avspublications.org/jvstb/about/rights_and_permissions

TGA indicated that the onset of oxidation for the Zn particles occurs at ~250 °C. HIM imaging revealed that a variety of ZnO nanostructures were formed for increasing annealing temperatures, particularly for larger particles. This is likely due to the differential thermal expansion of Zn core with respect to the ZnO outer shell, which led to the fracture of the ZnO shell and rapid oxidation of the Zn metal vapor that passed through these defects. Micro-XRD analysis of the films indicated the presence of both Zn and ZnO phases for samples annealed at lower temperatures, with increasing intensity of ZnO diffraction peaks and decreasing intensity of Zn diffraction peaks for increasing temperature. The micro-XRD data were used to estimate the relative compositions of metallic Zn and ZnO of the films, which were then used to calculate the thickness of the ZnO outer shell with annealing temperatures up to 600 °C. However, electrical characterization of the TFTs fabricated with Zn particle and ZIO precursors were dominated by the conducting nature of the thick Zn particle films. Due to the high surface to volume ratio of the Zn particles and the resulting ZnO nanostructures, the fabricated devices have the potential for application as field effect sensors to detect the adsorption of gas/liquid molecules due to variations in electrical conductivity.

ACKNOWLEDGMENTS

The Oregon Nanoscience and Microtechnologies Institute (ONAMI) funded this work. A portion of the work was performed at the Environmental Molecular Sciences Laboratory, a national scientific user facility sponsored by the Department of Energy's Office of Biological and Environmental Research, located at Pacific Northwest National Laboratory (PNNL), Richland, WA. PNNL is operated for the U.S. DOE by Battelle Memorial Institute under Contract No. DE-AC05-76RL01830. M.S.R. thanks PNNL for providing an Alternate Sponsored Fellowship.

[1]B. Sun and H. Sirringhaus, Nano Lett. **5**, 2408 (2005).
[2]B. L. Zhu, C. S. Xie, A. H. Wang, J. Wu, R. Wu, and J. Liu, J. Mater. Sci. **42**, 5416 (2007).
[3]Z. L. Wang, Appl. Phys. A. **88**, 7 (2007).
[4]L. Luo, Y. Zhang, S. S. Mao, and L. Lin, Sens. Actuators, A **127**, 201 (2006).
[5]S. A. Shojaee, M. M. Shahraki, M. A. F. Sani, A. Nemati, and A. Yousefi, J. Mater. Sci.: Mater. Electron. **21**, 571 (2010).
[6]S. Lee, Y. Jeong, S. Jeong, J. Lee, M. Jeon, and J. Moon, Superlattices Microstruct. **44**, 761 (2008).
[7]S. Kim, M.-C. Jeong, B.-Y. Oh, W. Lee, and J. M. Myoung, J. Cryst. Growth **290**, 485 (2006).
[8]T. Minami, H. Nanto, and S. Takata, Appl. Phys. Lett. **41**, 958 (1982).
[9]Y. I. Alivov, A. V. Chernykh, M. V. Chukichev, and R. Y. Korotkov, Thin Solid Films **473**, 241 (2005).
[10]W. S. Khan, C. Cao, G. Nabi, R. Yao, and S. H. Bhatti, J. Alloy Compd. **506**, 666 (2010).
[11]J. J. Wu and S. C. Liu, Adv. Mater. **14**, 215 (2002).
[12]S. J. Lim, S. Kwon, and H. Kim, Thin Solid Films **516**, 1523 (2008).
[13]Y. S. Kim, W. P. Tai, and S. J. Shu, Thin Solid Films **491**, 153 (2005).
[14]L. Znaidi, G. J. A. A. Soler Illia, S. Benyahia, C. Sanchez, and A. V. Kanaev, Thin Solid Films **428**, 257 (2003).
[15]B. Sun, R. L. Peterson, H. Sirringhaus, and K. Mori, J. Phys. Chem. C **111**, 18831 (2007).
[16]H.-C. Huang and T.-E. Hsieh, Nanotechnology **21**, 295707 (2010).
[17]S. T. Meyers, J. T. Anderson, C. M. Hung, J. Thompson, J. F. Wager, and D. A. Keszler, J. Am. Chem. Soc. **130**, 17603 (2008).
[18]H. C. Cheng, C. F. Chen, and C. C. Lee, Thin Solid Films **498**, 142 (2006).
[19]Y. W. Chen, Q. Qiao, Y. C. Liu, and G. L. Yang, J. Phys. Chem. C **113**, 7497 (2009).
[20]T. Y. Kim, J. Y. Kim, K. M. Senthil, E. K. Suh, and K. S. Nahm, J. Cryst. Growth **270**, 491 (2004).
[21]C. F. Guo, Y. Wang, P. Jiang, S. Cao, J. Miao, Z. Zhang, and Q. Liu, Nanotechnology **19**, 445710 (2008).
[22]X. Y. Kong, Y. Ding, and Z. L. Wang, J. Phys. Chem. B **108**, 570 (2004).
[23]Y. Gui, C. Xie, Q. Zhang, M. Hu, J. Yu, and Z. Weng, J. Cryst. Growth **289**, 663 (2006).
[24]S. Y. Han, G. S. Herman, and C.-H. Chang, ECS Trans. **33**, 275 (2010).
[25]S. Y. Han, G. S. Herman, and C.-H. Chang, J. Am. Chem. Soc. **133**, 5166 (2011).
[26]R. Nakamura, J. G. Lee, D. Tokozakura, H. Mori, and H. Nakajima, Mater. Lett. **61**, 1060 (2007).
[27]R. Wu, C. Xie, H. Xia, J. Hu, and A. Wang, J. Cryst. Growth **217**, 274 (2000).
[28]R. Wu, C. Xie, J. Hu, H. Xia, and A. Wang, Scr. Mater. **43**, 841 (2000).
[29]L. Gunawan and G. P. Johari, J. Phys. Chem. C **112**, 20159 (2008).
[30]W. K. Tan, K. A. Razak, K. Ibrahim, and Z. Lockman, J. Alloy Compd. **509**, 6806 (2011).
[31]H. J. Pandya and S. Chandra, J. Nano. Electron. Phys. **3**, 409 (2011).
[32]Y. G. Wang, S. P. Lau, H. W. Lee, S. F. Yu, and B. K. Tay, J. Appl. Phys. **94**, 354 (2003).

Downloaded 14 Sep 2012 to 128.193.163.10. Redistribution subject to AVS license or copyright; see http://avspublications.org/jvstb/about/rights_and_permissions